ECC
Eurasian Chemical Communications
Original Research Article
http://echemcom.com

Synthesis and characterization of nano α-Fe_2O_3/$Mn_2P_2O_7$ for photocatalytic decomposition of *p*-xylene using Box-Behnken design

Sajjad Mafi, Kazem Mahanpoor*

[a]*Department of Chemistry, Arak Branch, Islamic Azad University, Arak, Iran*

Received: 13 October 2019, Accepted: 02 November 2019, Published: 23 November 2019

Abstract

α-Fe_2O_3/$Mn_2P_2O_7$ photocatalyst was synthesized by forced hydrolysis and reflux condensation (FHRC) method. In order to fully evaluate the structure, chemical composition and morphology of synthesized composite, various analyses such as XRD, FT-IR, BET, EDX, SEM were applied. In this research, para-xylene was selected as the model substance for photocatalytic reactions to evaluate catalytic ability. To investigate the effect of parameters and select the optimum condition for the understudied process, Box Behnken Design (BBD) due to the Response Surface Methodology (RSM) was performed. For this purpose, catalyst concentration, hydrogen peroxide concentration, initial p-Xylene concentration and, pH were selected as important and effective variables. Results showed that the optimized degradation efficiency was close to 96.68% within 90 min. Based on the results, it was found that the initial concentration of *p*-Xylene had the greatest effect on the removal of contamination. Moreover, it was determined that the photocatalytic efficiency of the synthesized composite is more favorable than the non-supported α-Fe_2O_3.

Keywords: Photocatalyst; FHRC; $Mn_2P_2O_7$; *p*-Xylene; Box Behnken design.

Introduction

Increasing the amount of volatile organic compounds (VOCs) has become one of the environmental challenges of today. These compounds have harmful effects, such as damage to the ozone layer and the greenhouse effect [1]. VOCs usually emit from different sources such as printing and coating facilities, foundries, chemical industries, electronics, and paint manufacturing. Xylene is an example of this type of compound. It is a clear, colorless and hydrophobic liquid that has a characteristic smell [2]. This compound is usually applied as a solvent in printing, rubber, synthetic fiber, plastic, insecticide, pesticides and leather industries, and as a cleaner and a paint thinner [3]. Xylene is toxic to the liver, kidneys and the central nervous system when it comes into contact with skin or breathing system [4]. Isomers of xylene can be found in the list of hazardous and toxic atmospheric contaminants under

*Corresponding author: Kazem Mahanpoor
Tel: +98 (86) 33412608, Fax: +98 (86) 33412608
E-mail: k-mahanpoor@iau-arak.ac.ir

CAAA (Clean Air Act Amendments of 1990, USA).

Among different methods such as incineration, condensation, adsorption, absorption, ozonation and membrane separation technologies, photocatalysis is a very advanced strategy to degrade VOCs, due to its unique properties, including good efficiency, high mineralization, non-toxicity and easy accessibility [5]. In chemistry, photocatalysis is the acceleration of a photoreaction in the presence of a catalyst. In catalyzed photolysis, light is absorbed by an adsorbed substrate. In photogenerated catalysis, the photocatalytic activity (PCA) depends on the ability of the catalyst to create electron-hole pairs, which generate free radicals (e.g. hydroxyl radicals: •OH) able to undergo secondary reactions such as decomposition of pollutants [6].

Recently, much attention has been directed toward the production of nanoparticles [7], especially magnetic nanoparticles [8]. Iron (III) oxide or ferric oxide is the inorganic compound with the formula Fe_2O_3. It has many applications in the field of pigment production, catalysis, and medicine [9]. It is one of the three main oxides of iron. Fe_2O_3 has four polymorphs of α-, β-, ε-, and γ-Fe_2O_3. Among them, due to its cost-effectiveness, stability, eco-friendly and visible light harvesting ability, hematite (α-Fe_2O_3) as an n-type semiconductor with narrow band gap (2.0-2.2 eV), is widely used for photocatalytic degradation of pollutants. However, the point that should be noted is that these photocatalytic particles accumulate without any support, which decreases surface area and ultimately reduces photocatalytic activity.

Pyrophosphate (PPi), as an inorganic compound, is a diphosphate tetra-anion ($P_2O_7^{4-}$, $[O_3P\text{-}O\text{-}PO_3]^{4-}$) which has attracted a lot of attention due to its versatile coordination modes, low toxicity and biocompatibility [10]. Among them, manganese pyrophosphate, $Mn_2P_2O_7$, has been found to have an effective catalytic effect on the oxidative dehydrogenation of hydrocarbons and has also interesting magnetic properties at different temperatures, and it has been recommended as a standard material for magnetic susceptibility measurements [11]. However, here the manganese pyrophosphate was used to immobilize α-Fe_2O_3 nanoparticle.

In the present work, the composite of α-Fe_2O_3 nanoparticle and manganese pyrophosphate were synthesized using the Forced Hydrolysis and Reflux Condensation (FHRC) method. In order to make a comprehensive evaluation, the synthesized structure was investigated using characterization methods such as XRD, FTIR, EDAX, BET, and SEM. The synthesis of this compound results in the improvement of photocatalytic properties as well as the recyclability of the catalytic system. In order to investigate the different parameters of the photocatalytic process, *i.e.* the initial concentration of *p*-Xylene, the initial concentration of H_2O_2, concentration of catalyst and pH, Box-Behnken design (BBD) due to the Response Surface Methodology (RSM) was performed. A response surface methodology (RSM) might be applied to mapping a design space using a relatively small number of experiments. RSM provided an estimate of the response values for any possible combination of variables by modifying the number of involved factors in parallel.

The design method of response surface methodology is as follows [12]:

1. Designing a series of experiments for appropriate and

dependable measurement of the response of interest
2. Expanding a mathematical model of the second-order response surface with the best fittings
3. Exploring the optimal set of experimental parameters that generate a maximum or minimum value of the response
4. Demonstrating the direct and interactive effects of process parameters using two and three-dimensional graphs

Generally, a second-order model is used in response surface methodology [13].

$$\boldsymbol{y} = \boldsymbol{\beta_0} + \sum_{i=1}^{k} \boldsymbol{\beta_i x_i} + \sum_{i=1}^{k} \boldsymbol{\beta_{ii}\, x_i^2} + \sum_{i=1}^{k-1} \sum_{j=2}^{k} \boldsymbol{\beta_{ij} x_i x_j} + \boldsymbol{\varepsilon} \quad (1)$$

In the aforementioned equation $\boldsymbol{x_1}$, $\boldsymbol{x_2}$, …, $\boldsymbol{x_k}$ are the input factors which influence the response $\boldsymbol{y}$; $\boldsymbol{\beta_0}$, $\boldsymbol{\beta_{ii}}$ (i = 1, 2, . .., k), $\boldsymbol{\beta_{ij}}$ (i = 1, 2, . . ., k; j = 1, 2, . . . , k) are unknown parameters and $\boldsymbol{\varepsilon}$ is a random error. The $\boldsymbol{\beta}$ coefficients, which must be quantified in the second-order model, are obtained by the least square method. Generally, Eq. 1 can be written in matrix form as follows:

$$\boldsymbol{y} = bX + \boldsymbol{\varepsilon} \quad (2)$$

where $\boldsymbol{y}$ can be defined to be a matrix of measured values and X is a matrix of independent variables. In general, the matrixes b and $\boldsymbol{\varepsilon}$ consist of coefficients and errors, respectively.

Experimental

Materials

Iron (III) chloride hexahydrate was purchased from Daejung Company (Korea). Urea, ethylene glycol, EtOH (96%) and phosphorus pentasulfide (P_2S_5), manganese powder, and p-Xylene were purchased from Merck (Germany). Hydrogen peroxide (30%) was purchased from Chem Lab Company (Belgium).

Synthesis of manganese pyrophosphate ($Mn_2P_2O_7$)

Manganese pyrophosphate was synthesized in solvothermal condition and through the reaction between Mn metal powder and P_2S_5 species. Initially, 0.002 mol of Mn and 0.002 mol of P_2S_5 precursors were mixed with 30 mL of ethylene glycol in a Teflon-lined stainless steel autoclave. The autoclave was completely sealed and placed at 190 °C for 24 h. After this period, the autoclave was allowed to cool down to room temperature. The resultant was centrifuged to collect carefully from the reaction medium and then the separated precipitate was rinsed with distilled water and ethanol. After the synthesis of $Mn_2P_2O_7$, in order to evaluate its properties and prepare the considered nano-photocatalyst, manganese pyrophosphate was dried-up at 60 °C in a vacuum oven.

In the synthesis step of the pyrophosphate species, ethylene glycol also plays a reactant role in addition to the solvent. The reactions carried out during the synthesis of manganese pyrophosphates are as follows:

$$HOCH_2CH_2OH \rightarrow CH_3CHO + H_2O \quad (3)$$

$$P_2S_5 + 8H_2O \rightarrow 5H_2S + 2H_3PO_4 \quad (4)$$

$$2Mn + 2H_3PO_4 \rightarrow Mn_2P_2O_7 + H_2O + 2H_2 \quad (5)$$

The overall reaction will be as follows:

$$2Mn + P_2S_5 + 7HOCH_2CH_2OH \rightarrow Mn_2P_2O_7 + 7CH_3CHO + 5H_2S + 2H_2 \quad (6)$$

Synthesis of α-Fe_2O_3 /$Mn_2P_2O_7$ nano-photocatalyst using FHRC method

Initially, 50 mL iron (III) chloride hexahydrate with a concentration of 0.25 M was poured into a beaker. In the next step, 4 g $Mn_2P_2O_7$ was added slowly under vigorous agitation. The resulting mixture was stirred for 4-5 h. In the next step, stirring was stopped to allow solids to be precipitated. The separated solid transferred into a 50 mL flask. After stirring the solution in the flask, 50 mL urea 1 M was gradually added to it. The mixture was maintained at 90 °C for 12 h under reflux condition. The obtained precipitate after separation was washed with a 1:1 solution of ethanol to deionized water to remove unreacted ions. The resultant was maintained at room temperature for 2 h and then dried at 80 °C for 2 h. Finally, the calcination process was carried out at 300 ° C for 1 h.

General procedure for photocatalytic degradation of p-xylene

The overall schematic of the used photocatalytic reactor is shown in Figure 1. For each experiment, 250 mL of p-xylene was introduced into the reactor. The amount of p-xylene removal as the pollutant species is determined using the following equation:

$$\boldsymbol{X}\% = \frac{\boldsymbol{COD_0 - COD_t}}{\boldsymbol{COD_0}} \times \mathbf{100} \quad (7)$$

where COD_0 was the p-xylene concentration at time zero and COD_t was the corresponding amount at time t.

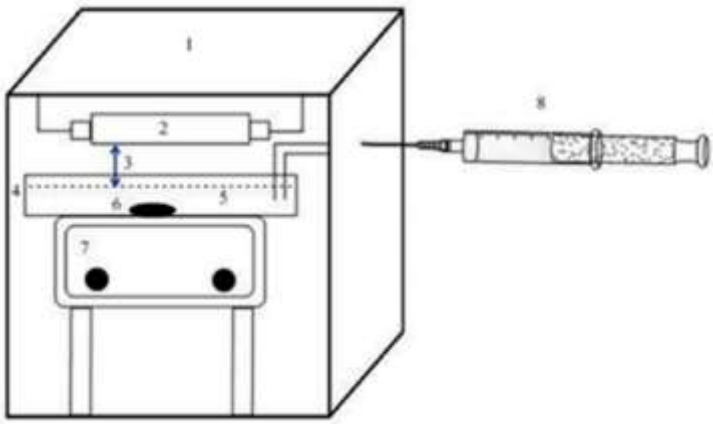

Figure 1. Schematic of the photocatalytic reactor. 1 MDF box, 50 × 50 × 50 cm; 2 Mercury lamps, Philips 15 W; 3 The distance between the surface of p-xylene solution and lamps, 5 cm; 4 Reactor, 300 mL capacity; 5 p-xylene solution, 250 mL; 6 Magnet; 7 Magnetic stirrers; 8 Sampling port.

Characterization methods

Powder X-ray diffraction (PXRD) patterns of the synthesized samples were recorded on a D5000 Siemens model diffractometer using Cu Kα radiation (40 kV and 40 mA).

FT-IR spectra were recorded on a Thermo Avatar spectrometer using the KBr pellet technique in order to identify the solid powder samples.

Scanning electron microscopy (SEM) images were obtained on the A Philips XL30 scanning electron microscope system.

In order to identify and determine the amount of existing elements, EDAX measurement was performed using FESEM (TESCAN) apparatus.

The textural property was measured using N_2 adsorption-desorption isotherms method on the BET–BJH specific surface area measurement equipment (Micromeretics ASAP 2010 system).

The Chemical Oxygen Demands (COD) were measured by COD Meter and Multiparameter Photometer (Hanna-HI83214).

Evaluation of photocatalytic performance

In this research, the design of experiments for the degradation process of p-Xylene was performed using Box-Behnken model. Four independent variables of pH, the concentration of hydrogen peroxide, the concentration of catalyst, and the initial concentration of p-Xylene, in three levels (-1, 0, +1) were tested and shown in Table 1.

Table 1. Experimental range and levels of the independent variables

Independent variables	Range of levels		
	-1	0	+1
pH	5	7	9
H_2O_2 con. (ppm)	0.1	0.3	0.5
Catalyst con. (ppm)	60	90	120
Initial con. of p-Xylene (ppm)	70	100	130

The number of experiments obtained using Box–Behnken model was determined as follows:

$$N = 2K (K-1) + C_0 \quad (8)$$

where N is the number of experiments, K is the number of variables, and C_0 is the number of central point's [14]. Table 2 shows the details of the performed Box–Behnken design of the experiment.

Table 2. Experimental conditions for the photocatalytic process

Exp. no.	Variables			
	pH	H_2O_2 con. (ppm)	Catalyst con. (ppm)	Initial con. of p-Xylene (ppm)
1	-1	-1	0	0
2	1	-1	0	0
3	-1	1	0	0
4	1	1	0	0
5	0	0	-1	-1
6	0	0	1	-1
7	0	0	-1	1
8	0	0	1	1
9	-1	0	0	-1
10	1	0	0	-1
11	-1	0	0	1
12	1	0	0	1
13	0	-1	-1	0
14	0	1	-1	0
15	0	-1	1	0
16	0	1	1	0
17	-1	0	-1	0
18	1	0	-1	0
19	-1	0	1	0
20	1	0	1	0
21	0	-1	0	-1
22	0	1	0	-1
23	0	-1	0	1
24	0	1	0	1
25	0	0	0	0
26	0	0	0	0

27	0	0	0	0

Results and discussion

FT-IR spectroscopy

In order to determine the composition of the surface, the FT-IR method was used. Figure 2 represents the FT-IR spectra of pristine $Mn_2P_2O_7$ and synthesized α-$Fe_2O_3/Mn_2P_2O_7$ composite, which prepared using FHRC method. In the FT-IR spectrum of synthesized $Mn_2P_2O_7$, there was a strong absorption for $Mn_2P_2O_7$ sample at 1094 cm^{-1}, which was ascribed to asymmetric stretching of PO_2 unit. The bands at 736 cm^{-1} and 950 cm^{-1}, which were appeared in the pristine $Mn_2P_2O_7$ materials spectrum was due to the stretching vibration of P-O bond and symmetric or asymmetric stretching mode of P-O-P tertiary group, respectively [15]. The bands at 1600 cm^{-1} and 3500 cm^{-1} in the spectrum of the synthesized composite were related to bending and stretching vibrating modes of O-H bond, respectively. The peaks at around 482 cm^{-1} and 886 cm^{-1} were ascribed to vibration mode of Fe-O bond [16]. Other changes in the spectral range from 400 to 500 cm^{-1} represents the formation of new bonds in the synthesized composite.

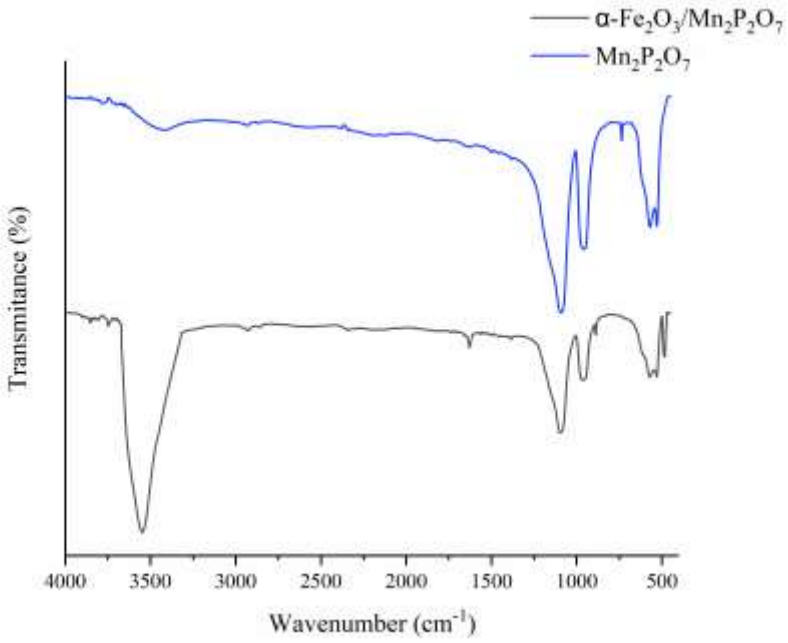

Figure 2. FT-IR spectra of synthesized compounds

Powder X-ray diffraction

XRD pattern of the synthesized α-$Fe_2O_3/Mn_2P_2O_7$ composite was displayed in Figure 3. This pattern exhibited (111), (-201), (130), (131) and (-311) Bragg reflections at 2θ = 28.96, 30.36, 34.41, 41.61 and 43.71, which were in good agreement with powder diffraction data and attributed to the monoclinic structure of $Mn_2P_2O_7$. Furthermore, some additional peaks were observed for the synthesized α-$Fe_2O_3/Mn_2P_2O_7$ composite at 2θ = 24.11, 33.06, 35.66, 49.26 and 54.0 which were assigned to planes of (012), (104), (110), (024) and (116) in the rhombohedral (hexagonal) structure of α-Fe_2O_3 (space group: R-3c) [17].

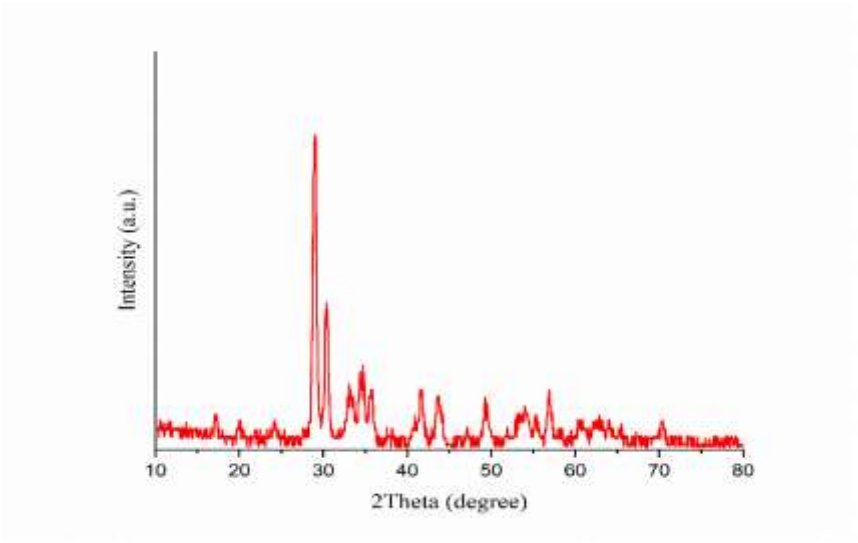

Figure 3. XRD pattern of synthesized α-Fe_2O_3/$Mn_2P_2O_7$

Scanning electron microscopy

The morphology of synthesized composite was investigated using SEM technique (Figure 4). The SEM image of the prepared α-Fe_2O_3/$Mn_2P_2O_7$ nanocomposite displayed that the surface of $Mn_2P_2O_7$, which acts as the support for the photocatalyst, was obviously decorated by numerous metal oxide particles with a typical diameter of less than 90 nm. The catalytic α-Fe_2O_3 nanoparticles, which were synthesized using the FHRC method, were dense and close to each other on the surface.

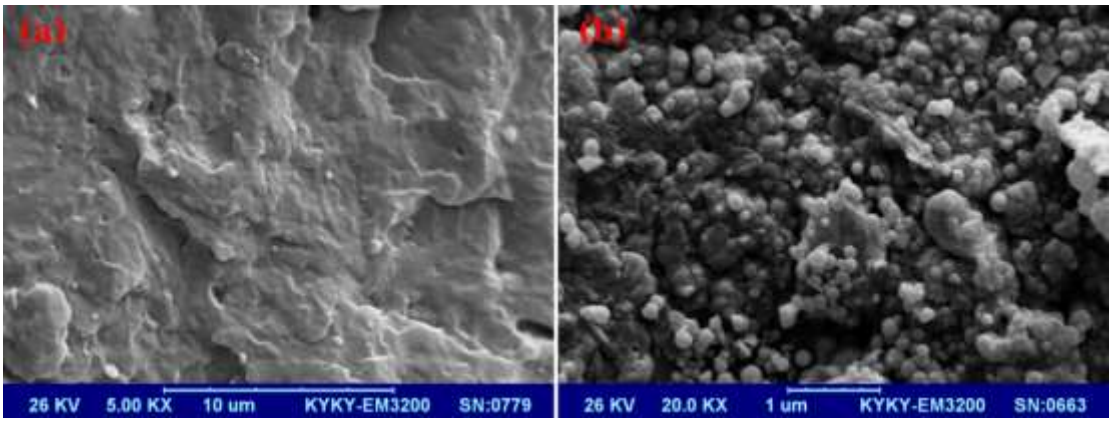

Figure 4. SEM images of (a) synthesized $Mn_2P_2O_7$ and (b) synthesized α-Fe_2O_3/$Mn_2P_2O_7$ composite

Energy dispersive X-ray analysis

EDX method was used to detect the presence of the elements and also to determine the amount of them in the synthesized composite. Figure 5 shows the EDX spectrum of the synthesized composite. The obtained spectrum proves the presence of oxygen, phosphorus, iron and manganese elements in the synthesized composite. These obtained data and values confirmed that α-Fe_2O_3/$Mn_2P_2O_7$ composite was formed.

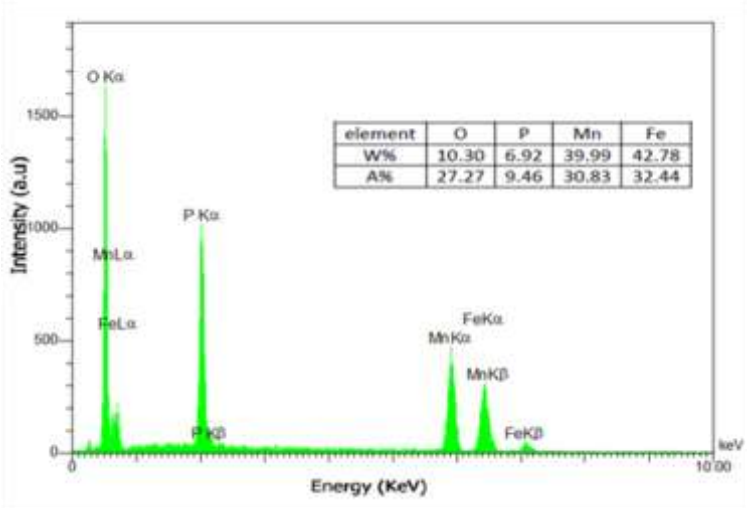

Figure 5. EDX spectrum of the synthesized composite

Surface area measurement using the BET method

The specific surface areas of the α-Fe_2O_3/$Mn_2P_2O_7$ composite and $Mn_2P_2O_7$ have been measured. The obtained isotherms are shown in Figure 6. The adsorption-desorption isotherms of these materials showed a hysteresis loop classified as type IV by IUPAC. The specific surface area of the solid support was 125 m^2/g. when the composite was formed, the surface area increased to 160 m^2/g. This increase in surface area is due to the presence of the α-Fe_2O_3 nanoparticles on the surface of $Mn_2P_2O_7$.

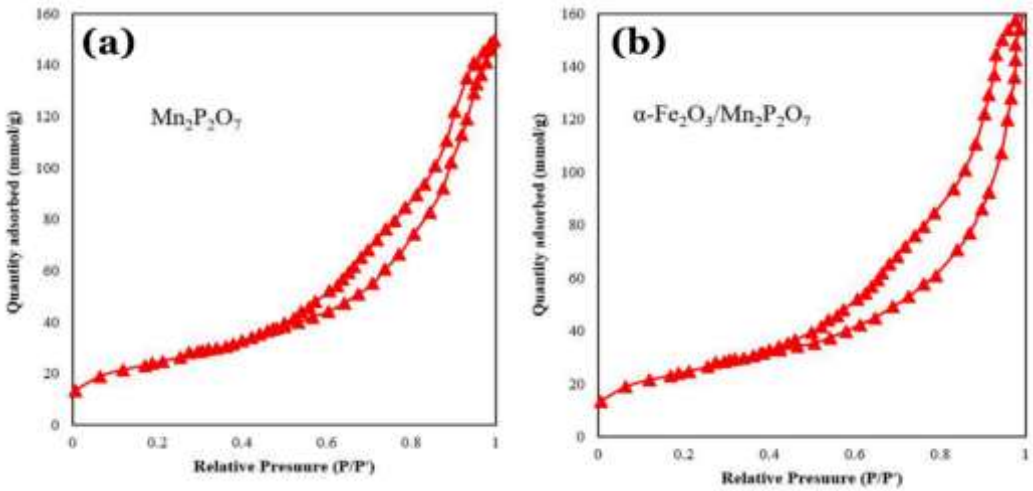

Figure 6. Adsorption-desorption isotherms of (a) synthesized $Mn_2P_2O_7$ and (b) α-Fe_2O_3/$Mn_2P_2O_7$ composite

In accordance with the results presented in the literature [18], a schematic of the proposed photocatalytic mechanism is shown in Figure 7 and the main stages are numbered. In the first stage, the photons from the UV light are absorbed by the α-Fe_2O_3 photocatalyst, which causes the electrons in the valence band to be transferred to the conduction band and thus form electron-hole pairs. In the second step, some electrons and holes are recombined again and the energy is lost in the form of heat. The third stage is the beginning of the process of oxidation by the cavities in the valence band that produce hydroxyl radicals. In the fourth stage, the

reduction process is performed by excited electrons, which are placed in the conduction band. Finally, photocatalytic reactions are conducted to decompose contaminants and produce mineral products. In this way, hydroxyl radicals attack to the contaminating molecules and degrade them chemically. The process details are summarized in the following chemical equations:

$\alpha\text{-}Fe_2O_3 + h\nu \rightarrow \alpha\text{-}Fe_2O_3\,(e^- CB + h^+vb)$

$h^+vb + H_2O_{(ads)} \rightarrow H^+ + {}^oOH^-_{(ads)}$

$h^+vb + OH^-_{(ads)} \rightarrow {}^oOH_{(ads)}$

$e^- CB + O_{2\,(ads)} \rightarrow {}^oO_2^-{}_{(ads)}$

$H_2O \rightleftharpoons H^+ + OH^-$

${}^oO_2^-{}_{(ads)} + H^+ \rightarrow {}^oHO_2$

$2\,{}^oHO_2 \rightarrow H_2O_2 + O_2$

$H_2O_2 + \alpha\text{-}Fe_2O_3\,(e^- CB) \rightarrow {}^oOH + OH^- + \alpha\text{-}Fe_2O_3$

${}^oOH_{(ads)}$ + p-Xylene → Degradation of p-Xylene

h^+vb + p-Xylene → Oxidation of p-Xylene

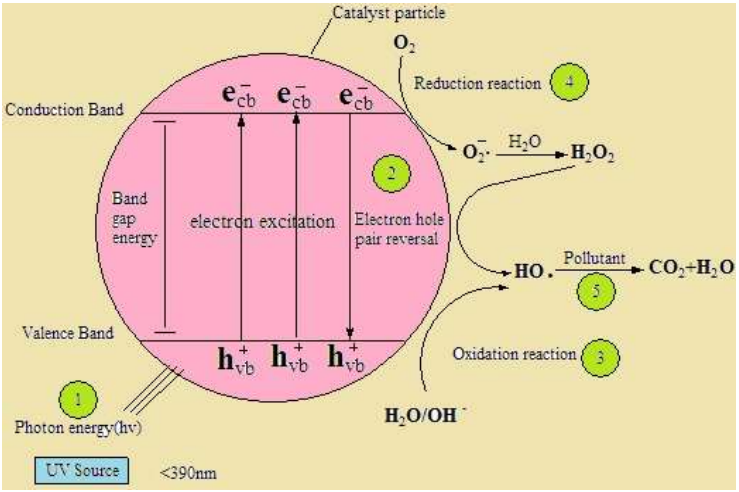

Figure 7. A proposed mechanism of the photocatalytic process

Design of experiments and statistical analysis

Analysis of variance (ANOVA) is a collection of a number of statistical methods used in the analysis of the difference between the mean of groups and the related methods. ANOVA is used to test the meaningfulness of the mean of three or more variables. Also, this method is used for graphical data analysis to obtain the interaction between process variables and response. The quality of the polynomial model is expressed through the coefficient of determination of R_2 and the significance of the coefficients is determined using F-test (Fisher test). The components of the model are evaluated through P-Value. Table 3 presents the estimated effects and coefficients of each model component for the response variable (X%). In this table, the standard error of estimation (S), coefficient of determination (R_2), adjusted coefficient of determination (R_2 adjusted) and prediction coefficient (R_2 Pred) have also been reported. The square of the correlation coefficient is calculated as the coefficient of determination (R_2) for the response variable. The accuracy and diversity of the model are evaluated through R_2. The value of R_2 is always between 0 and 1. When R_2 is close to 1, indicate higher power of the model in the determination of the X% variable and its better prediction. In this research, the obtained value of R_2 was 99.55%.

According to Table 3 and the significant effect of variables on the process, the magnitude of the effects of pH, concentration of H_2O_2, concentration of catalyst and Initial concentration of p-Xylene variables were obtained -2.908, 1.287, 4.145, and -14.89, respectively. Therefore, the reaction parameters (from highest to lowest effect) were p-Xylene concentration, catalyst concentration, pH and H_2O_2 concentration, respectively. It should be noted that despite the two variables of H_2O_2 concentration and catalyst in the model, the effect of pH (-2.908) and concentration of p-Xylene (-14.89) was negative in the model. It means that increasing the initial concentration of p-Xylene or pH will result in reduced efficiency. In this way, the interactive effects of variables are reported in Table 3.

Table 3. Coefficient effects for actual degradation (%)

Term	Coef	SE Coef	T (Coef/SE Coef)	P value	Result
Constant	78.41	0.628	124.9	0.000	Significant
pH	-2.908	0.314	-9.27	0.000	Significant
H_2O_2 con.	1.287	0.314	4.1	0.001	Significant
Catalyst con.	4.145	0.314	13.2	0.000	Significant
Initial con. of P-Xylene	-14.89	0.314	-47.43	0.000	Significant
pH×pH	-0.556	0.471	-1.18	0.260	
H_2O_2 con. × H_2O_2 con.	0.799	0.471	1.7	0.116	
Catalyst con. × Catalyst con.	-0.089	0.471	-0.19	0.854	
Initial con. of P-Xylene × Initial con. of P-Xylene	-4.556	0.471	-9.68	0.000	Significant
pH × H_2O_2 con.	-0.893	0.544	-1.64	0.127	
pH × Catalyst con.	-0.227	0.544	-0.42	0.683	
pH × Initial con. of P-Xylene	0.544	1.55	0.146	1.000	
H_2O_2 con. × Catalyst con.	-1.442	0.544	-2.65	0.021	Significant
H_2O_2 con. × Initial con. of P-Xylene	0.095	0.544	0.17	0.864	
Catalyst con. × Initial con. of P-Xylene	1.83	0.544	3.37	0.006	Significant

S=1.087, R^2=99.55%, Adj R^2=99.03%, Pred R^2=97.44%

As can be seen, the only dual interaction between the catalyst and the concentration of p-Xylene has a positive effect on the response. The second-order effects of P-Xylene × P-Xylene and the interaction of H_2O_2 × Catalyst in the model are negative and significant. It should be noted that the obtained P-values for each of the model components in Table 3 are measured according to the considered error level ($\alpha = 0.05$). Table 4 shows the results of the ANOVA. The effect of each parameter on the response variable increases with increasing F-value and decreasing the P-value. For the main effects (with 4 degrees of freedom), including the initial concentration of P-Xylene, pH, H_2O_2 concentration and catalyst concentration, F and P values were determined to be 631.77 and P <0.0001, respectively. In addition, F and P values for second-order effects were 31.27 and P <0.0001 respectively and for interactive interactions, values of 3.95 and 0.021 were obtained.

Table 4. ANOVA results

Source	Degree of Freedom	Adj SS	Adj MS	F Value	P Value
Model	14	3163.96	226.00	191.13	0.000
pH	1	101.50	101.50	85.84	0.000
H_2O_2 con.	1	19.87	19.87	16.80	0.001
Catalyst con.	1	206.17	206.17	174.36	0.000
Initial con. of P-Xylene	1	2660.55	2660.55	2250.08	0.000
pH×pH	1	1.65	1.65	1.40	0.260
H_2O_2 con. × H_2O_2 con.	1	3.40	3.40	2.88	0.116
Catalyst con. × Catalyst con.	1	0.04	0.04	0.04	0.854
Initial con. of P-Xylene × Initial con. of P-Xylene	1	110.72	110.72	93.64	0.000
pH × H_2O_2 con.	1	3.19	3.19	2.69	0.127
pH × Catalyst con.	1	0.21	0.21	0.18	0.683
pH × Initial con. of P-Xylene	1	2.86	2.86	2.42	0.146
H_2O_2 con. × Catalyst con.	1	8.32	8.32	7.04	0.021
H_2O_2 con. × Initial con. of P-Xylene	1	0.04	0.04	0.03	0.864
Catalyst con. × Initial con. of P-Xylene	1	13.40	13.40	11.33	0.006
Error	12	14.19	1.18		
Lack-of-Fit	10	14.08	1.41	26.03	0.038
Pure Error	2	0.11	0.05		
Total	26	3178.15			

Table 5. Residual values

Exp. no.	Actual %	Predicted %	Residual (X%-fit)	St resid
1	79.22	79.38	-0.16	-0.23
2	76.45	75.35	1.10	1.57
3	83.45	83.74	-0.29	-0.41
4	77.11	76.14	0.97	1.38
5	85.78	86.34	-0.56	-0.80
6	91.17	90.97	0.20	0.28
7	53.51	52.90	0.61	0.87
8	66.22	64.85	1.37	1.95
9	93.38	91.94	1.44	2.05
10	84.11	84.43	-0.32	-0.46
11	61.27	60.47	0.80	1.14
12	55.38	56.34	-0.96	-1.37
13	72.61	72.25	0.36	0.52
14	78.69	77.70	0.99	1.40
15	82.91	83.42	-0.51	-0.73
16	83.22	83.11	0.11	0.16
17	75.35	76.30	-0.95	-1.35
18	70.49	70.94	-0.45	-0.64
19	84.21	85.05	-0.84	-1.19
20	78.44	78.77	-0.33	-0.48
21	88.22	88.35	-0.13	-0.19
22	90.11	90.73	-0.62	-0.89
23	57.72	58.38	-0.66	-0.94
24	59.99	61.14	-1.15	-1.64
25	78.45	78.41	0.04	0.05
26	78.16	78.41	-0.25	-0.28
27	78.62	78.41	0.21	0.24

Table 5 contains additional results, which were used for the residual plot. As can be seen, the actual and predicted values are very close together. Another method, which is very useful for checking the distribution of residues is plotting the normal probability plot (P-plot). If the distribution of residues is normal, the plot is similar to a straight line.

Figure 8 (a) shows the normal probability plot. In this plot, it is clear that the distribution of residues is normal due to the fact that all the points are close to the straight line. If the model is correct and if the assumptions have been met, the residues should not have a particular trend. In particular, they should not correlate with any other variables including the fitted variables. The evaluation of this issue carried out using the plot of the residual values against fitted values.

Figure 8 (b) shows the plot of residues against fitted values. As can be seen, the residual plot versus the fitted values has non-uniformity and does not show any particular trend. According to Figure 8 (C), the abundance diagram of residual values indicates the relatively normal distribution of the residuals. In order to better understand the residual values, the residual plot is shown against the observed values in Figure 8 (d). As seen, 15 points (residues) are located below the line (negative) and 12 points above the line. According to this point and comparing the distance from the zero line, it can be stated that the distribution of the residues is normal. The mathematical model that shows the efficiency of p-Xylene removal in this research is given in the following Equation:

$$\text{Degradation\%} = \mathbf{82.5} + \mathbf{0.10}(\boldsymbol{pH}) + \mathbf{30.1}(\boldsymbol{H_2O_2}) + \mathbf{0.051}(\boldsymbol{Cat}) + \mathbf{0.230}(\mathbf{p-xylene}) - \mathbf{0.139}(\boldsymbol{pH})^2 + \mathbf{20.0}(\boldsymbol{H_2O_2})^2 - \mathbf{0.000099}(\boldsymbol{Cat})^2 - \mathbf{0.005062}(\mathbf{p-xylene})^2 - \mathbf{2.32}(\boldsymbol{pH} \times \boldsymbol{H_2O_2}) - \mathbf{0.00379}\,(\boldsymbol{pH} \times \boldsymbol{Catalyst}) + \mathbf{0.01408}(\boldsymbol{pH} \times \mathbf{p-xylene}) - \mathbf{0.2404}(\boldsymbol{Cat} \times \boldsymbol{H_2O_2}) + \mathbf{0.0158}(\boldsymbol{H_2O_2} \times \mathbf{p-xylene}) + \mathbf{0.002033}(\boldsymbol{Cat} \times \mathbf{p-xylene})$$

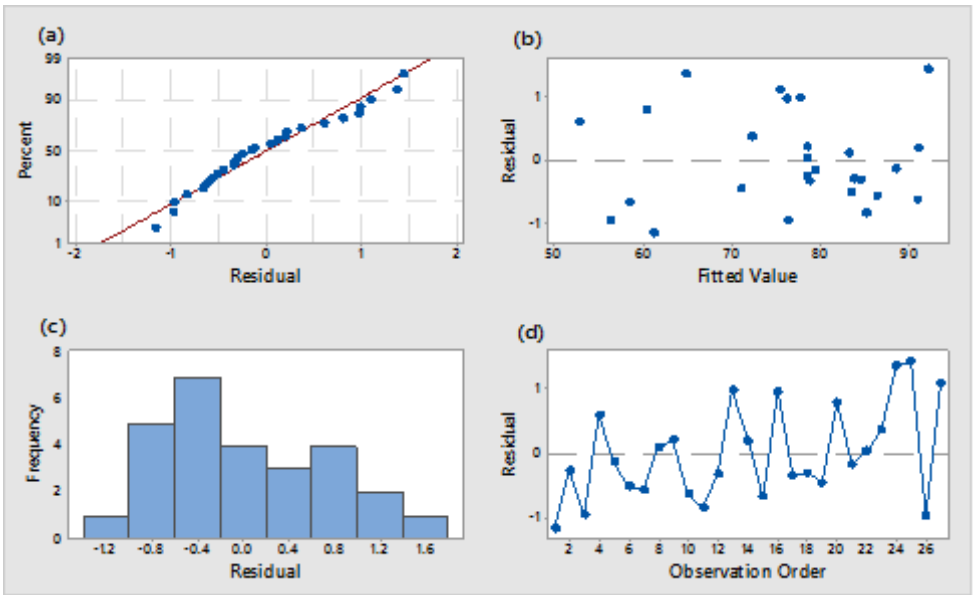

Figure 8. (a) Normal probability plot, (b) plot of residuals versus fitted values, (c) Histogram of residuals, (d) plot of residuals versus observation order

Figure 9 shows the main effects graphs. Based on these graphs, from the four main parameters, the effect of two pH and p-Xylene parameters on the response variable (p-Xylene removal efficiency) is negative. The effect of two catalysts and H_2O_2 parameters is positive. The slope of the line in the main graph is an indicator of the magnitude of independent variable effects on the process. Therefore, the effective variables are p-Xylene, catalyst, pH and H_2O_2, respectively.

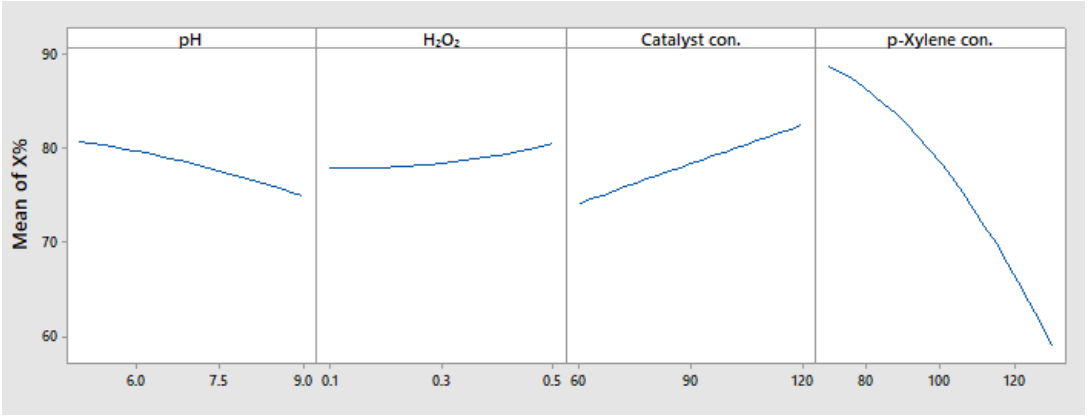

Figure 9. Main effect plot for actual degradation (%)

In Figure 10, the interactive effects of variables on the efficiency of xylene removal have been investigated. As can be seen, there is a significant interactive effect between catalyst concentration and H_2O_2 concentration. In addition, there is a higher interactive effect between the catalyst and the concentration of p-Xylene.

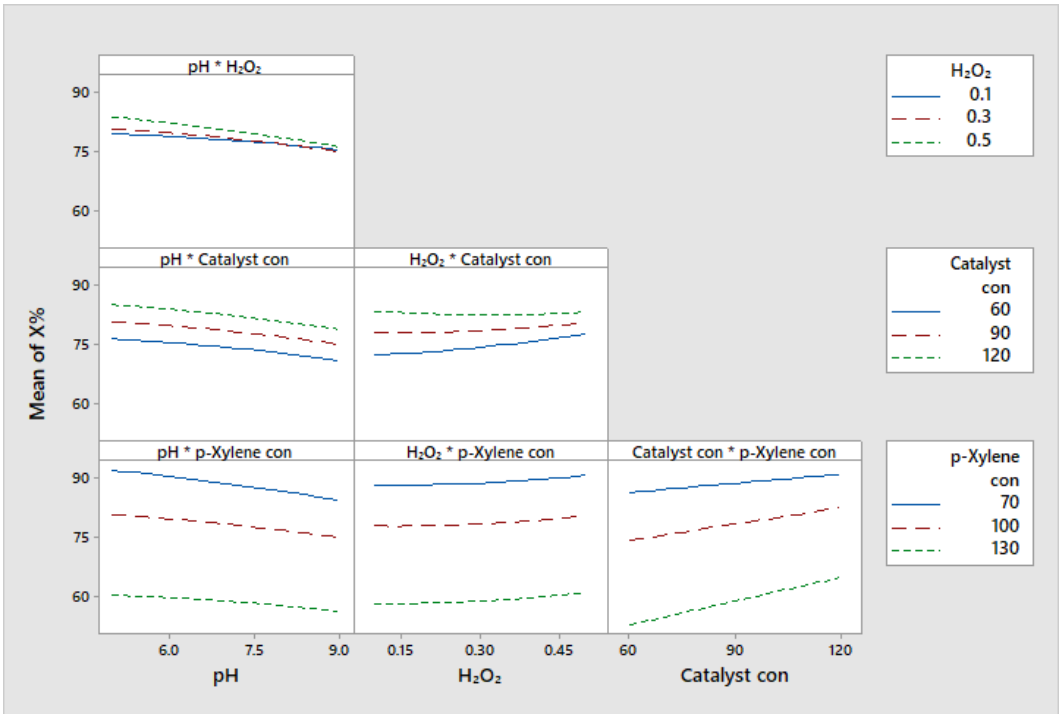

Figure 10. Interaction plot for actual degradation (%)

It is easy to detect the optimum condition of the experiment through plotting response surface and contour graphs. Figure 11 shows the response level graph for the experiment variables. Figure 11 (a) shows the three-dimensional response graph of the resulting regression model, assuming a constant pH and H_2O_2 concentration in values of 7 and 0.3 ppm, respectively. As seen in this figure, the highest removal efficiency occurs at a concentration of 120 ppm of catalyst and a concentration of 70 ppm P-Xylene. In addition, by reducing the concentration of catalyst and increasing the concentration of p-Xylene, the efficiency of the removal of p-Xylene decreases. Figure 11 (b) shows the three-dimensional graph, assuming a constant pH and catalyst in values of 7 and 90 ppm, respectively. The optimum removal point for P-xylene concentration is 70 ppm and for H_2O_2 concentration is 0.5 ppm .The results also indicate that the removal efficiency is more dependent on P-Xylene than on H_2O_2 concentration .Figure 11 (c) shows the three-dimensional response surface graph with the assumption of constant pH and p-Xylene in the values of 7 and 100 ppm, respectively. The most effective removal of p-Xylene, in this case, occurred in the catalyst concentration of 120 ppm and H_2O_2 of 0.5 ppm. Figure 11 (d) shows the three-dimensional response graph, with the assumption that H_2O_2 and catalyst are kept constant in the values of 0.3 ppm and 90 ppm, respectively. In the pH of 5 and p-Xylene concentration of 70 ppm, the most effective removal of p-Xylene occurs. Moreover, Figure 11 (e) illustrates the three-dimensional graph with the assumption that H_2O_2 and p-Xylene are kept constant at values of 0.3 ppm and 100 ppm, respectively. The results showed that the highest efficiency for xylene removal in a pH of 5 and catalyst concentration of 120 ppm was obtained. Figure 11 (f) shows the three-dimensional response graph of the resulting regression model, assuming a constant catalyst and P-Xylene concentration in values of 90 ppm and 100 ppm, respectively. The most effective removal of xylene is achieved in pH values of 5 and H_2O_2 concentration of 0.5 ppm.

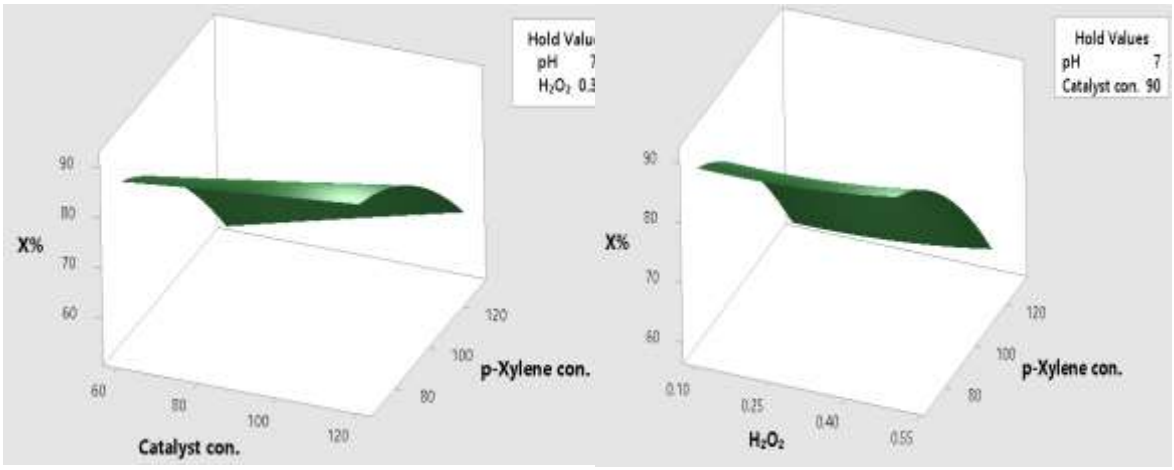

a **b**

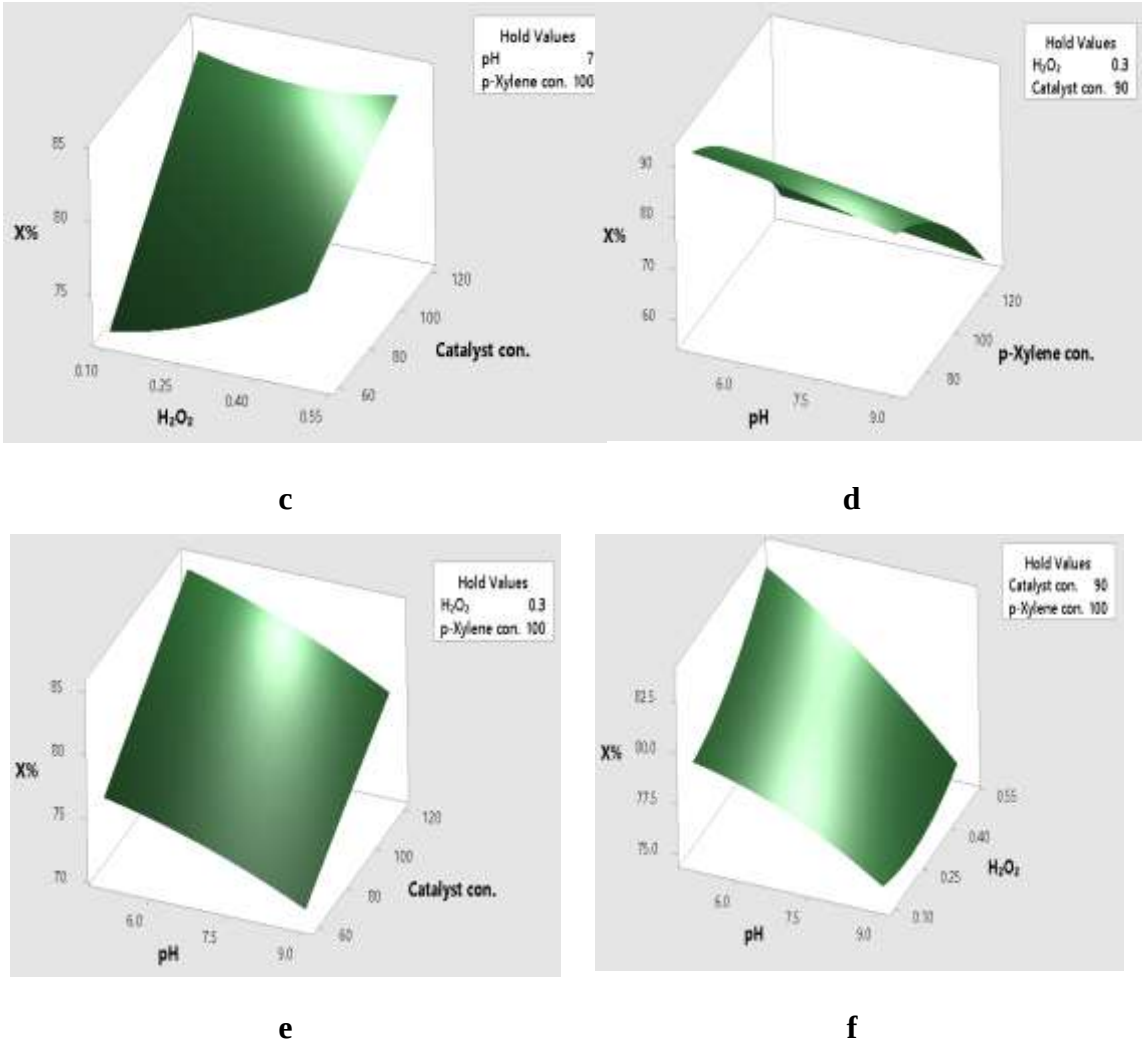

Figure 11. The surface plot for actual degradation (%)

The results of the contour graphs are shown in Figure 12. The Figure 12 (a) shows the changes in the efficiency of p-Xylene removal by maintaining the pH and H_2O_2 at levels of 7 and 0.3. As can be seen, with the increase in the amount of p-Xylene, the efficiency of removal is reduced and by increasing the amount of catalyst, the efficiency is increased. Figure 12 (b) shows the changes in the efficiency of the p-Xylene removal by keeping the pH and catalyst values constant at levels of 7 and 90 ppm. According to the results, with a decrease in the amount of P-Xylene, removal efficiency is increased. In addition, the efficiency of the removal of p-Xylene, in the range of 0.1 to 0.4 ppm of H_2O_2 concentration, remains constant. While the utilized amount of H_2O_2 was 0.5 ppm, removal efficiency increased. Figure 12 (c) shows the changes in the efficiency of the p-Xylene removal by keeping the pH and P-Xylene concentration fixed at levels of 7 and 100. The results indicate that by increasing the catalyst and H_2O_2 concentrations, the efficiency of the p-Xylene removal increases. Figure 12 (d) shows the changes in the efficiency of the p-Xylene removal by keeping the two variables of H_2O_2 and catalyst fixed at the levels of 0.3 ppm and 90 ppm. The results indicate that by decreasing the pH and p-Xylene values,

the efficiency of the removal process increased. Figure 12 (e) shows the changes in the efficiency of p-Xylene removal by keeping the two variables of H_2O_2 and P-Xylene fixed at levels of 0.3 ppm and 100 ppm. The results indicate that by decreasing the pH and increasing the catalyst concentration, process efficiency increases. Figure 12 (f) shows the changes in the efficiency by keeping the two variables of catalyst and p-Xylene fixed at 90 ppm and 100 ppm. As can be seen, the efficiency of p-Xylene removal increases with decreasing pH and increasing the amount of H_2O_2.

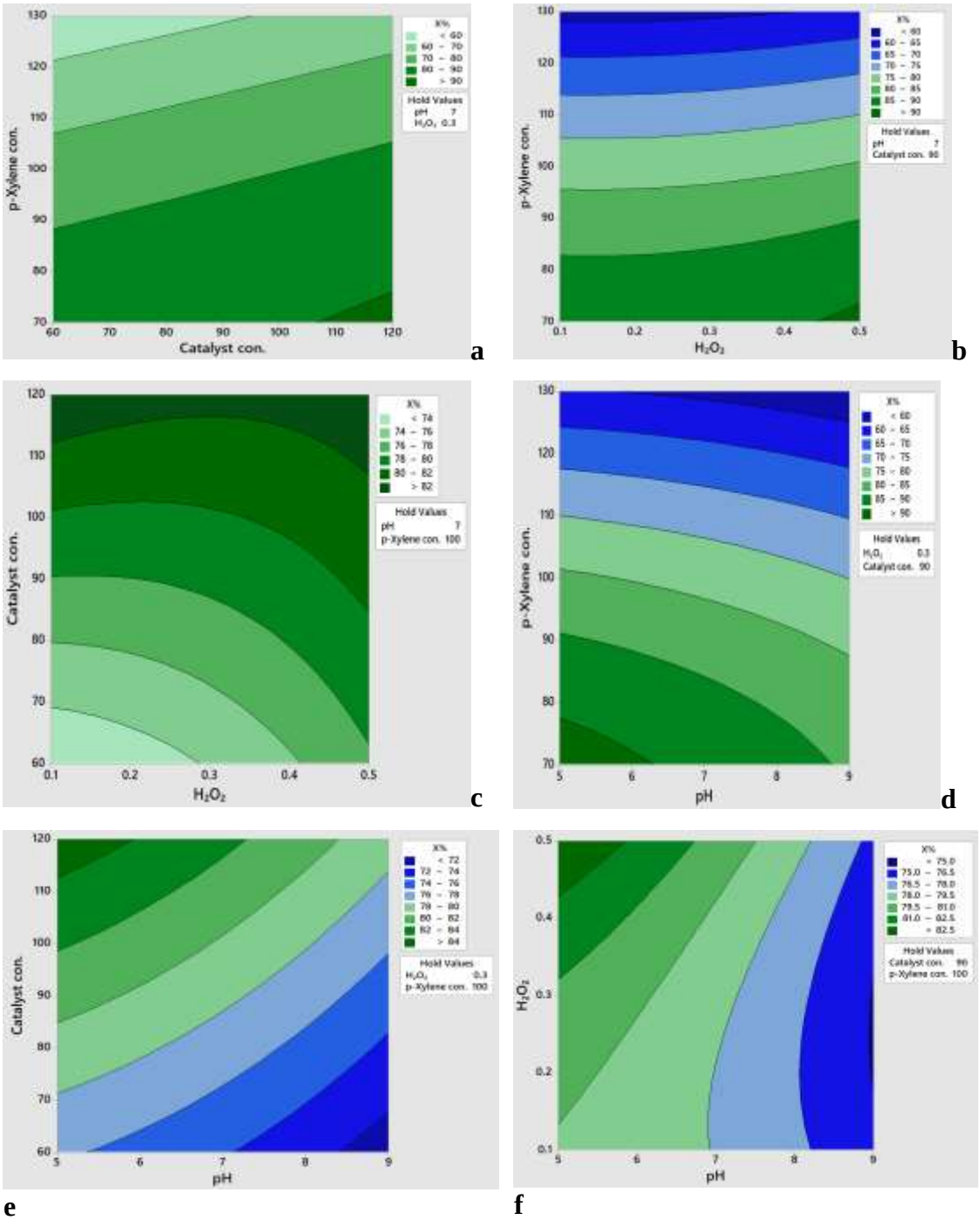

Figure 12. Contour plot for actual degradation (%)

In order to fully evaluate and investigate the effect of support on the photocatalytic activity, pure α-Fe_2O_3 was also used. For this purpose, all of 27 experiments that were designed for the α-Fe_2O_3/$Mn_2P_2O_7$ composite were also studied for the pure α-Fe_2O_3 species. The obtained results, which are summarized in Table 6 shows that α-Fe_2O_3/$Mn_2P_2O_7$ composite has better performance than α-Fe_2O_3 species in the degradation process of p-Xylene. This indicates that the presence of the $Mn_2P_2O_7$ support prevents the particles aggregation. Therefore, the presence of support will increase the surface area of the photocatalytic nanoparticles.

Table 6. Comparison between the performance of α-Fe_2O_3/$Mn_2P_2O_7$ composite and pure α-Fe_2O_3

Exp. No.	Actual efficiency %	
	Pure α-Fe_2O_3	**α-Fe_2O_3 / $Mn_2P_2O_7$**
1	69.89	79.22
2	65.13	76.45
3	72.61	83.45
4	67.14	77.11
5	74.15	85.78
6	83.82	91.17
7	40.41	53.51
8	55.83	66.22
9	85.23	93.38
10	72.77	84.11
11	53.54	61.27
12	45.43	55.38
13	62.32	72.61
14	67.41	78.69
15	71.54	82.91
16	72.31	83.22
17	61.22	75.35
18	60.98	70.49
19	73.17	84.21
20	67.97	78.44
21	79.55	88.22
22	81.42	90.11
23	47.21	57.72
24	51.78	59.99
25	67.23	78.45
26	67. 45	78.16
27	67.92	78.62

Optimization of conditions

The exact values of the optimal variables are shown in Table 7. In order to assess the accuracy of the prediction, that was performed using the Minitab 18 software, p-Xylene removal process was performed in the predicted optimal conditions (*i.e.*; pH=5, C_{H2O2}=0.5 ppm, $C_{Catalyst}$=120 ppm, and $C_{p\text{-}Xylene}$=70 ppm). The experimental result obtained in optimal conditions was 96.68% for p-Xylene removal, which was close to the predicted value of 95.84%. The proximity between the experimental and the predicted values represents the validity of the existing model. This shows that RSM is a powerful tool for determining the exact values of the optimal conditions [19].

Table 7. The optimum value of the process parameters

pH	C_{H2O2} (ppm)	$C_{Catalyst}$ (ppm)	$C_{p\text{-}Xylene}$ (ppm)	Efficiency (%)	
				Actual	Predicted
5	0.5	120	70	96.68	95.84

Conclusion

In summary, α-Fe_2O_3/$Mn_2P_2O_7$ composite as an efficient photocatalyst was prepared using forced hydrolysis and reflux condensation method (FHRC). Based on the results of XRD, EDAX, FT-IR, BET, and SEM, it was found that α-Fe_2O_3 nanoparticles were decorated on the $Mn_2P_2O_7$ surface. AOPs (α-Fe_2O_3/$Mn_2P_2O_7$, UV/H_2O_2) as a solution-based method was used to investigate the photodegradation process of p-Xylene. Results of the photocatalysis experiment showed that the photodegradation efficiency appeared to reach 96.68% in 90 min. According to the literature, it can be suggested that ^{o}OH species are the most effective agents, which control the reaction mechanism. In comparison with non-supported α-Fe_2O_3 nanoparticles, the heterogeneous system had better performance due to the distribution of particles on the surface of the manganese pyrophosphate that prevents the accumulation of nanoparticles. The heterogeneity and recyclability of the photocatalyst system, along with the proper efficiency of the catalyst, are the most important features of the synthesized catalyst.

Acknowledgments

The authors thank the Arak Azad University for laboratory facilities.

References

[1] D. Wu, X. Quan, Y. Zhao, S. Chen, *J. Hazard. Mater.*, **2006**, *136*, 288-295.
[2] (a) H. Hong-Sheng, S. Hao, Z. Ya-Jin, *Commun. Theor. Phys.*, **2013**, *59*, 443-446; (b) M. Almasi, *Chem. Methodol.*, **2018**, *2*, 308-314; (c) A. Khazaei, M.A. Zolfigol, M. Mokhlesi, F.D. Panah, S. Sajjadifar, *Helvetica Chimica Acta*., **2012**, *95*, 106-114.
[3] H. Elmrini, N. Bredin, Z. Shareefdeen, M. Heitz, *Chem. Eng. J.*, **2004**, *100*, 149-158.
[4] B. Bühler, B. Witholt, B. Hauer, A. Schmid, *Appl. Environ. Microbiol.*, **2002**, *68*, 560-568.
[5] (a) H. Salavati, A. Teimouri, S. Kazemi, *Chem. Methodol.*, **2017**, *2*, 158-169; (b) H. Salavati, A. Teimouri, S. Kazemi, *Chem. Methodol.*, **2017**, *1*, 12-27; (c) C. Ye, K. Hu, Z. Niu, Y. Lu, L. Zhang, K. Yan, *J. Water. Process. Eng.*, **2019**, *27*, 205-210.
[6] M. Mishra, D.-M. Chun, *Appl. Catal. A. Gen.*, **2015**, *498*, 126-141.
[7] (a) W.E. John, A.A. Ayi, C. Anyama, P.B. Ashishie, B.E. Inah, *Adv. J. Chem. A.*, **2019**, *2*, 175-183; (b) S. Deljoo, N. Rabiee, M. Rabiee, *Asian J. Nanosci. Mater.*, **2019**, *2*, 66-91; (c) P. Gharbani, A. Mehalizadeh, *Asian J. Nanosci. Mater.*, **2019**, *2*, 27-36.
[8] (a) F. Moeinpour, A. Khojastehnezhad, *Chin. Chem. Lett.*, **2015**, *26*, 575-579; (b) P. Torabian, F. Ghandehari, M. Fatemi, *Asian J. Green Chem.*, **2018**, *2*, 181-188; (c) E. Teymoori, A. Davoodnia, A. Khojastehnezhad, N. Hosseininasab, *Iran. Chem. Commun.*, **2019**, *7*, 271-282; (d) B. Maleki, N. Nasiri, R. Tayebee, A. Khojastehnezhad, H.A. Akhlaghi, *RSC Adv.*, **2016**, *6*, 79128-79134; (e) B. Maleki, M. Baghayeri, S.A.J. Abadi, R. Tayebee, A. Khojastehnezhad, *RSC Adv.*, **2016**, *6*, 96644-96661.

[9] (a) X. Li, C. Wang, Y. Zeng, P. Li, T. Xie, Y. Zhang, *J. Hazard. Mater.*, **2016**, *317*, 563-569; (b) J. Zou, J. Oladipo, S. Fu, A. Al-Rahbi, H. Yang, C. Wu, N. Cai, P. Williams, H. Chen, *Energy. Convers. Manag*., **2018**, *171*, 241-248; (c) E. Rafiee, S. Eavani, *Green Chem*., **2011**, *13*, 2116-2122.
[10] T.J. Greenfield, M. Julve, R.P. Doyle, *Coord. Chem. Rev.*, **2019**, *384*, 37-64.
[11] S. Wang, X. Jiang, G. Du, Z. Guo, J. Jang, S.-J. Kim, *Mater. Lett.*, **2011**, *65*, 3265-3268.
[12] P. Peasura, *Sci. World J.*, **2015**, *2015*, 1-8.
[13] (a) N. Tafreshi, S. Sharifnia, S.M. Dehaghi, *Process. Saf. Environ. Prot.*, **2017**, *106*, 203-210; (b) E. Ambrosio, D.L. Lucca, M.H. Garcia, M.T. de Souza, T.K. Souza. S. Freitas, R.P. de Souza, J.V. Visentainer, J.C. Garcia, *Sci. Total. Environ.*, **2017**, *581*, 1-9.
[14] (a) R. Zeynolabedin, K. Mahanpoor, *J. Nanostructure. Chem.*, **2017**, *7*, 67-74; (b) S. Sajjadifar, S.A. Mirshokraie, N. Javaherneshan, O. Louie, *American Journal of Organic Chemistry*, **2012**, *2*, 1-6.
[15] B. Boonchom, R. Baitahe, *Mater. Lett.*, **2009**, *63*, 2218-2220.
[16] M. Chen, J. Liu, D. Chao, J. Wang, J. Yin, J. Lin, H.J. Fan, Z.X. Shen, *Nano Energy.*, **2014**, *9*, 364-372.
[17] A. Lassoued, B. Dkhil, A. Gadri, S. Ammar, *Results Phys.*, **2017**, *7*, 3007-3015.
[18] (a) V. Augugliaroa, M. Bellarditaa, V. Loddoa, G. Palmisanoa, L. Palmisanoa, S. Yurdakalb, *J. Photochem. Photobiol. C. Photochem. Rev.*, **2012**, *13*, 224-245; (b) O. Mehraj, B.M. Pirzada, N.A. Mir, M.Z. Khan, S. Sabir, *Appl. Surf. Sci.*, **2016**, *387*, 642-651; (c) D. Zhao, G. Sheng, C. Chen, X. Wang, *Appl. Catal. B. Environ.*, **2012**, *111*, 303-308.
[19] (a) A. Shokri, F. Rabiee, K. Mahanpoor, *Int. J. Environ. Sci. Technol.*, **2017**, *14*, 2485-2494; (b) A. Shokri, K. Mahanpoor, D. Soodbar, *J. Environ. Chem. Eng.*, **2016**, *4*, 585-598.

How to cite this manuscript: Sajjad Mafi, Kazem Mahanpoor. Synthesis and characterization of nano α-Fe_2O_3/$Mn_2P_2O_7$ for photocatalytic decomposition of *p*-xylene using Box-Behnken design. *Eurasian Chemical Communications*, 2020, 2(1), 59-77.